Primate Horizontal Cell Dynamics: An Analysis of Sensitivity Regulation in the Outer Retina

Vivianne C. Smith, Joel Pokorny, Barry B. Lee and Dennis M. Dacey

J Neurophysiol 85:545-558, 2001.

Journal of Neurophysiology publishes original articles on the function of the nervous system. It is published 12 times a year (monthly) by the American Physiological Society, 9650 Rockville Pike, Bethesda MD 20814-3991. ISSN: 0022-3077, ESSN: 1522-1598. Visit our website at http://www.the-aps.org/.

Primate Horizontal Cell Dynamics: An Analysis of Sensitivity Regulation in the Outer Retina

VIVIANNE C. SMITH,[1] JOEL POKORNY,[1] BARRY B. LEE,[2] AND DENNIS M. DACEY[3]
[1]*Visual Sciences Center, University of Chicago, Chicago, Illinois 60637;* [2]*Max Planck Institute for Biophysical Chemistry, 37077 Gottingen, Germany; and* [3]*Department of Biostructure, University of Washington, Seattle, Washington 98175*

Received 13 March 2000; accepted in final form 12 October 2000

Smith, Vivianne C., Joel Pokorny, Barry B. Lee, and Dennis M. Dacey. Primate horizontal cell dynamics: an analysis of sensitivity regulation in the outer retina. *J Neurophysiol* 85: 545–558, 2001. The human cone visual system maintains sensitivity over a broad range of illumination, from below 1 troland to 1,000,000 trolands. While the cone photoreceptors themselves are an important locus for sensitivity regulation—or light adaptation—the degree to which they contribute in primates remains unclear. To determine the range of sensitivity regulation in the outer retina, the temporal dynamics, neural gain control, and response range compression were measured in second-order neurons, the H1 horizontal cells, of the macaque retina. Situated at the first synapse in the retina, H1 cells receive input from a large population of cones. Lee et al. have previously shown that sensitivity regulation in H1 cells is both cone type-specific and spatially restricted. The sensitivity regulation seen in H1 cells at moderate illuminances thus takes place before the summation of cone signals in these cells, and the data establish the H1 cell as a convenient locus for analyzing cone signals. In the present study, cone-driven responses of primate H1 cells to temporally modulated sine-wave stimuli and to increment pulses were measured at steady levels of 1–1,000 trolands. The H1 cell gave a modulated response to sine-wave stimuli and hyperpolarized to increment pulses with overshoots at stimulus onset and offset. The temporal amplitude sensitivity function was primarily low-pass in shape, with a small degree of low-frequency roll off and a resonance shoulder near 40 Hz. A model incorporating a cascade of first-order filters together with an underdamped second-order filter could describe both temporal sinusoidal and pulse hyperpolarizations. Amplitude sensitivity was estimated from both pulse and sine-wave data as a function of the steady adaptation level. Sensitivity at low light levels (1 troland) showed a slowing in temporal dynamics, indicating time-dependent sensitivity regulation. Sensitivity was reduced at light levels above approximately 10 trolands, reflecting both response range compression and neural gain control. Thus the outer retina is a major locus for sensitivity regulation in primates.

INTRODUCTION

The human cone pathways maintain psychophysical sensitivity to small increments of illumination ($\Delta I/I$) over a dynamic range greater than 6 decades, from 1 troland (td) to 1,000,000 td, a level at which 98% of the cone photopigment is isomerized (Hood and Finkelstein 1986). This dynamic range is obtained partially by sensitivity regulation (gain control) mechanisms that adjust the response to the steady illumination level, and partly by illumination-dependent changes in response dynamics that are faster with an increase in illumination. Sensitivity at low adaptation levels is proportionately higher because response continues to grow over a longer time period (Donner et al. 1995). At least some sensitivity regulation mechanisms act independently on the long- (L), middle- (M), and short- (S) wavelength-sensitive cone signals (Stiles 1978). Further, cone-type sensitivity regulation does not show spatial pooling, i.e., it occurs independently in neighboring cones (MacLeod et al. 1992). The implication is that a substantial amount of sensitivity regulation must occur in the outer retina.

The relationship between the properties of human light adaptation and the physiology of cones and their pathways is, however, unclear. In primates, it is difficult to record directly from cones in the intact retina. Initial electrophysiological studies using mass recording techniques (Boynton and Whitten 1970; Valeton and van Norren 1983) suggested that sensitivity regulation showed an onset near 140 td and did not reach Weber's law until light levels sufficient to cause photopigment depletion (c. 20,000 td) were reached. Measurements of the photocurrent in the outer segment of macaque cones (Schnapf et al. 1990) found evidence of sensitivity regulation onset at an even higher level, above an estimated 2,000 td. More recent voltage recordings from cone inner segments (Schneeweis and Schnapf 1999) have indicated a lower onset of 630 td. Neither study of isolated cones showed evidence of variation in response dynamics. Thus there is at least a 14–63-fold discrepancy in estimates of the onset of sensitivity regulation in primates between the psychophysical (10 td) and the electrophysiogical data (140 td) (Schneeweis and Schnapf 1999; Valeton and van Norren 1983). We were therefore concerned that previous electrophysiological estimates of sensitivity regulation in primates had underestimated both the range and the role of response dynamics governing sensitivity regulation.

In non-mammalian vertebrates, a calcium-dependent mechanism of gain control in the photoreceptor has been identified in the rod outer segment (Pugh and Lamb 1990). Intracellular recordings from intact cones in turtle (Burkhardt 1994; Normann and Anderton 1983; Normann and Perlman 1979) have shown that factors including gain control, illumination-dependent response dynamics, response range compression, and pigment depletion provide a Weber's law slope over a nearly seven-decade illuminance range. About 3.3 log units of this

Address for reprint requests: D. Dacey, Dept. of Biological Structure, University of Washington, Box 357420, Seattle, WA 98195-7420 (E-mail: dmd@u.washington.edu).

The costs of publication of this article were defrayed in part by the payment of page charges. The article must therefore be hereby marked "*advertisement*" in accordance with 18 U.S.C. Section 1734 solely to indicate this fact.

range are below bleaching levels (i.e., 10–20,000 td). A calcium-dependent mechanism of gain control similar to that of rods is an attractive candidate to explain such data (Burkhardt 1994).

Our goal was to measure temporal dynamics, sensitivity regulation, and response range compression of cone signals in primate horizontal (H) cells, which receive direct input from a large population of cones. The horizontal cell is a suitable locus for study of sensitivity regulation initiated in the cones. Sensitivity regulation in horizontal cells is both cone type-specific and spatially local, indicating that the sensitivity regulation measured in horizontal cells occurs prior to summation of cone signals in these cells (Lee et al. 1999). The source of such effects includes the outer segment transduction cascade, inner segment ion channel interactions, and interactions in the cone pedicle that could modulate the flow of transmitter. Horizontal cells are large and provide stable responses for many hours in the living in vitro retinal preparation. There are two types of horizontal cell in the primate retina. One of them, the H1 type, receives summed input from the L and M cones and lacks significant S-cone input. Light absorbed by L or M cones evokes a hyperpolarizing response. The other, the H2 type, receives summed input from all cone types, with the S cone providing a particularly strong input (Dacey et al. 1996). Here our studies were restricted to the H1 type.

We used illuminance conditions designed to measure cone responses by maintaining an illumination above 1 td on the retina and by avoiding periods of full dark adaptation, conditions under which no rod response is present in H1 cells (Verweij et al. 1999). We measured H1 cell responses both to temporal sinusoids and to pulsed stimuli. These two protocols offer differing advantages, but to the extent that the initial H1 cell response to light at any steady illumination shows linear systems behavior, they should give identical estimates of temporal dynamics and sensitivity. The advantage of the sine-wave stimulus is that it provides a data set that is easily modeled by a linear systems approach. The available contrasts are low and this allowed us to work at a time average retinal illumination as high as 1,000 td. The advantage of the pulse stimulus is that it provides a greater range of contrasts to allow estimation of receptor saturation and hence response range compression. Our results demonstrate significant sensitivity regulation at the level of the H1 cell. We noted both adjustment of sensitivity to the steady-state illumination and variation in response dynamics with illumination level, providing increased sensitivity to test stimuli as low as 1 td.

METHODS

Preparation

The in vitro preparation of macaque retina has been previously described (Dacey 1994, 1996). In brief, eyes from *Macaca nemestrina* or *M. fascicularis* were obtained through the Tissue Distribution Program of the Regional Primate Research Center at the University of Washington and removed under deep barbiturate anesthesia just prior to death. Retinas were dissected free of the vitreous and sclera in oxygenated Ames' medium (Sigma) and the retina-choroid was placed flat, vitreal surface up, in a superfusion chamber mounted on the stage of a light microscope. Horizontal cell nuclei were identified following a 20-min superfusion of the nuclear stain 4,6-diamidino-2-phenylindole (DAPI; ~10 μM). Microelectrodes were filled with a solution of 2–3% Neurobiotin (Vector Labs, Burlingame, CA) and 1–2% pyranine (Molecular Probes, Eugene, OR) in 1 M KCl. Electrical impedances ranged from 200 to 300 MΩ. Pyranine fluorescence in the electrode and DAPI fluorescence in cells were viewed together under episcopic illumination. Penetration was confirmed by iontophoresis of pyranine into the cell. At the termination of recording, cells were preserved for later analysis by injection of Neurobiotin and subsequent horseradish peroxidase histochemistry after tissue fixation.

Optical equipment

Visual stimuli originated from two light-emitting diodes (LEDs) with peak wavelengths at 638 and 554 nm. The LEDs were mounted above the camera port of the microscope, their beams combined with dichroic mirrors and focused near the objective lens of the microscope to form a homogeneous field at the vitreal surface of the retina. Objects in the camera port were in focus on the retina, and apertures at this location regulated stimulus size. The LEDs were under computer-control, driven by a constant-amplitude frequency-modulated pulse train, giving a linear relation between light output and driving voltage. The 638 and 554 nm LEDs were set to equal luminance by flicker photometry by a human observer viewing the camera port image on the microscope stage. The setting was corrected for the absence of the ocular media (Wyszecki and Stiles 1982).

The LED outputs (μW cm^{-2}) were measured with a Gamma Scientific spectroradiometer placed in the image plane. LEDs were scanned in 2- to 5-nm steps through their spectral range. For the 554-nm LED, the calculated total quanta s^{-1} μm^{-2} at the retinal surface were 42,415 at the highest average illumination level (Wyszecki and Stiles 1982). For comparison with psychophysical studies, these units were converted into trolands, units of equivalent human retinal illuminance. This conversion used the Judd spectral luminous efficiency function and published formulae (Wyszecki and Stiles 1982). In the intact eye, photoreceptors are directed at the exit pupil (Enoch and Laties 1971; Laties and Enoch 1971) and show a dependence of absorption on the angle of incident light (the Stiles-Crawford effect, SCE). In the far peripheral retina of the flat-mount preparation, receptors are angled at ~45° relative to the stimulus light path. Thus the effective retinal illuminance is reduced. We estimated (Lee et al. 1999) from human SCE data that this angle would correspond to a sixfold decrease in the effective retinal illuminance compared with the calculation using formulae for the intact eye (Wyszecki and Stiles 1982). The equivalent average retinal illuminance for comparison with human psychophysics, taking into account this factor, was estimated at 500 td for the 554 nm LED. We validated our calculations by comparison of data collected in macaque retinal ganglion cells in intact (Lee et al. 1990) and in vitro recordings (Dacey and Lee 1994).

Data acquisition

The data were obtained using a custom-built acquisition system, a Macintosh Quadra 950 with National Instrument A/D boards with a resolution of 50 μV. Averaging improved the effective resolution to 5–10 μV. The resting membrane potential was measured at about −60 mV in the light-adapted state (1,000 td). Sine-wave temporal modulation and light pulses were employed as stimuli. For sine-wave stimuli, sampling rate ranged from 312.5 to 5 kHz with increasing stimulus frequency. Data were sampled at 3.2-ms intervals at 0.61 Hz (512 samples/cycle, 312.5 Hz) decreasing to 0.2 ms at 78 Hz (64 samples/cycle, 5 kHz). For pulses, sampling rate was 1 kHz.

Stimuli

Sine-wave data were obtained at several (usually 6) Michelson contrasts, $(I_{max} - I_{min})/(I_{max} + I_{min})$, between 0.0325 and 1.0 and at temporal frequencies from 0.61 to 78 Hz. About 6 s of activity were

averaged at each frequency. Data collection at higher frequencies continued until responses became smaller than about 50 μV. The LEDs were modulated temporally in phase, giving an average retinal illuminance of 1,000 td (500 td/LED). The response amplitudes were subject to Fourier analysis, and the first-harmonic amplitude and phase were determined. Pulse data were obtained at seven Weber contrasts ($I_{pulse}/I_{background}$) between 0.1 and 19, relative to a steady background. Both LEDs were used and the steady level was 100 td. Decrement pulses were used to obtain a measure of response range compression. Pulse durations ranged from 10 to 160 ms, using a 500-ms epoch (2.5-ms binwidth). Twenty stimulus repetitions were averaged for the pulse stimuli.

The illuminance level was changed by insertion of neutral density filters. After each decrease in retinal illuminance by a factor of 10, we allowed a few minutes to elapse to enable sensitivity to stabilize. The majority of data were collected with a stimulus diameter of about 5° on the retina (1,000 μm). Diameters between 1 (200 μm) and 15° (3,000 μm) were also used.

RESULTS

Our strategy was first to collect temporal sensitivity functions at a full range of frequencies to derive a linear systems model of the dynamics. Then we collected data for both pulses and a low frequency sine-wave in the same cells so as to compare neural sensitivity regulation estimated by the two protocols.

Sine-wave temporal stimulation

Data were obtained for seven cells for 20 frequencies and a 5° diameter stimulus. Figure 1 shows the first-harmonic amplitudes for one H1 cell plotted as a function of Michelson contrast for two temporal frequencies at the 1,000 td average retinal illuminance. The *insets* in the graph show the averaged raw traces with the - - - indicating the resting membrane potential level immediately before data collection. At contrasts below 0.25, responses were sinusoidal around the resting level. Response amplitudes increased linearly with contrast. The slope of the linear portion of the curve was estimated to yield contrast gain (mV/contrast) as a function of temporal frequency. These contrast responsivity data were then expressed in amplitude sensitivity (mV/retinal illuminance) in the plots of Figs. 2 and 3. The first-harmonic phase was independent of contrast (not shown) and phase was estimated from the 0.25 Michelson contrast data. At contrasts above 0.5, the response waveform was visibly distorted. The Fourier transform showed significant energy in the higher harmonics. At low frequencies (0.5–5 Hz), the distortion consisted of an asymmetry about the resting level, flattening of the hyperpolarization maximum, and a deep depolarization to the sine-wave minimum. As a result of this distortion, the Fourier first-harmonic amplitude tended to fall above the linear relation at low frequencies. At higher frequencies (10–40 Hz), a sawtooth-like distortion with a rapid depolarization segment was apparent, but Fourier first-harmonic amplitudes remained a linear function of contrast.

Amplitude sensitivity (mV/retinal illuminance) and phase are plotted as a function of temporal frequency for three H1 cells in Fig. 2. Three illuminance levels are shown for each cell. At 1,000 td, the temporal response was primarily low-pass in shape, with only a small roll-off at temporal frequencies below 5 Hz (Fig. 2, *A–C, top traces*). There was a slight shoulder at 40 Hz, indicative of a resonance peak. The amplitude sensitivity increased with illuminance decrease (Fig. 2, *A–C, top traces*) with an accompanying phase delay (Fig. 2, *A–C, bottom traces*). The shape of the temporal amplitude sensitivity function changed with a relative sensitivity loss in the mid-frequency range. The luminance-dependent phase lag was similarly greatest in this mid-frequency range. The high-frequency amplitude decline remained steep and continued to show a resonance shoulder. At high frequencies, the amplitude sensitivities converged toward a single line.

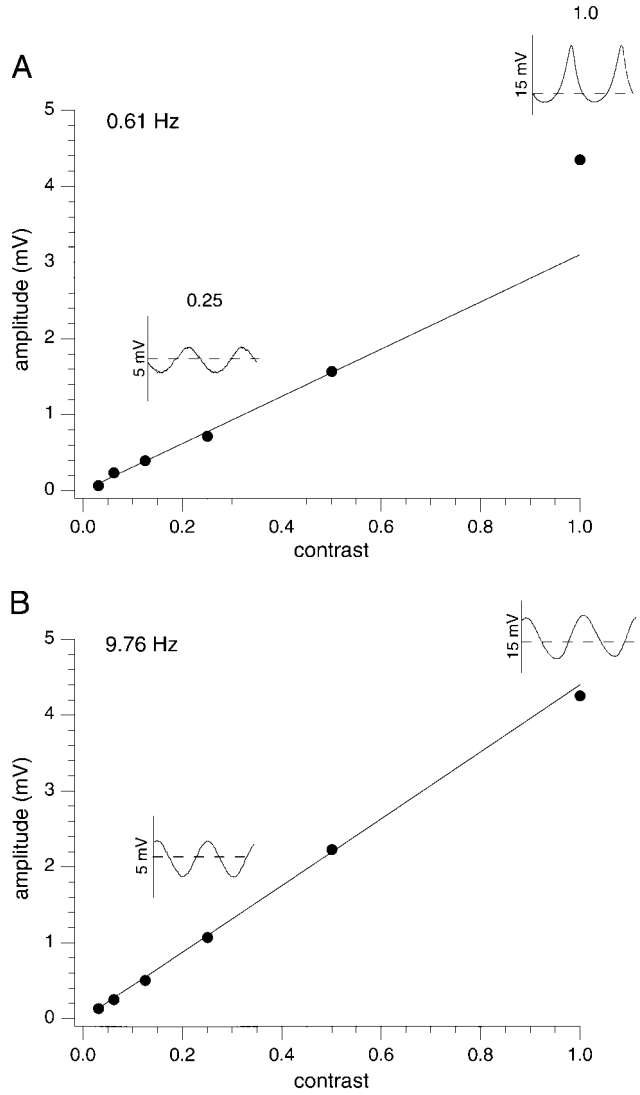

FIG. 1. First-harmonic amplitudes derived from Fourier analysis of averaged sine-wave responses of an H1 cell as a function of Michelson contrast at 0.61 Hz (*A*) and 9.76 Hz (*B*) for a 5° stimulus diameter. The time-average luminance was 1,000 trolands (td). —, fits to linear part of the data. *Insets*: average data traces at 0.25 and 1.0 Michelson contrasts.

The data shown in Fig. 2 were representative of all cells studied. There was inter-cell variation in amplitude sensitivity; the mean Fourier amplitude computed from the contrast gain functions (Fig. 1) at 0.61 Hz was 5.25 ± 1.1 (SD) mV/td at 1,000 td, 3.47 ± 1.0 mV/td at 100 td, and 0.89 ± 1.0 at 10 td. There was also variation in the amount of resonance but little variation in the amount of low-frequency roll-off or of the high-frequency cutoff. The phase was approximately $-\pi$ at low frequency, becoming more negative with increasing fre-

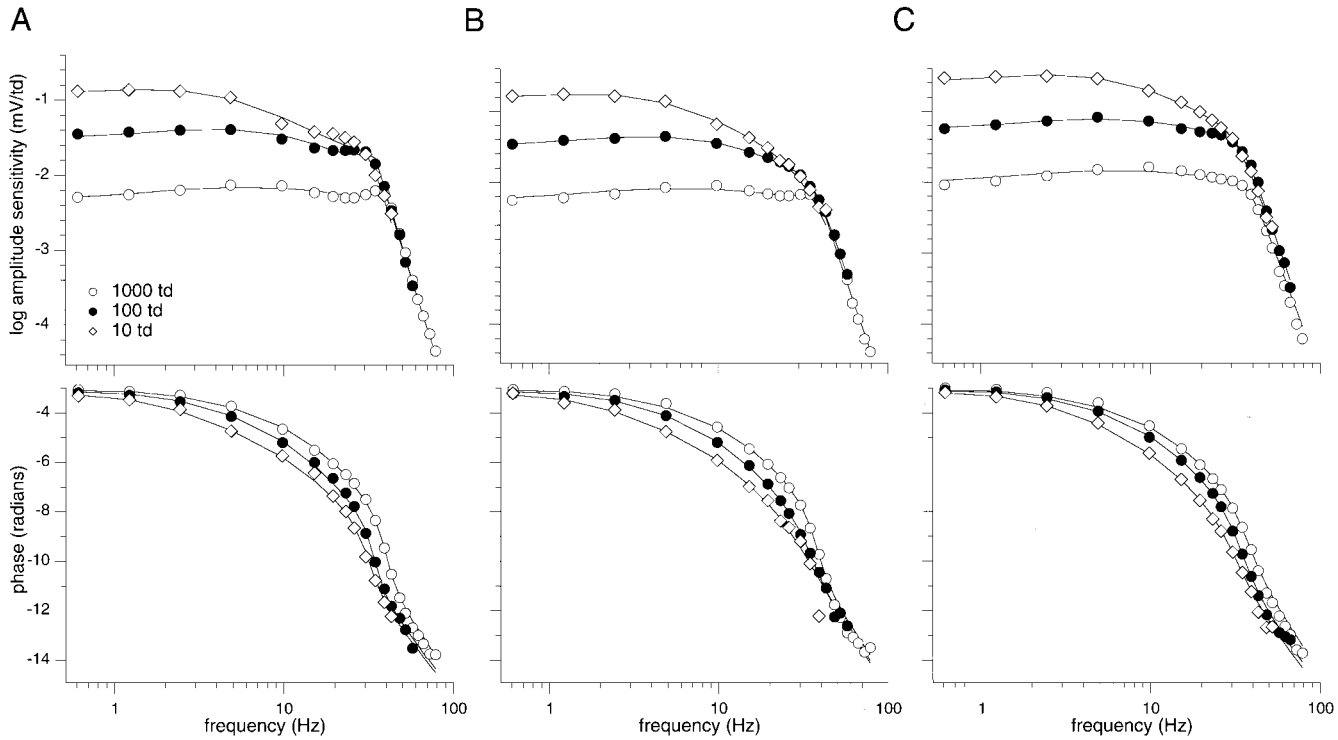

FIG. 2. Amplitude sensitivity in mV/retinal illuminance (*top traces*) and phase (*bottom traces*) plotted as a function of temporal frequency for 3 H1 cells (*A*, *B*, and *C*). Stimulus diameter was 5°. Data are shown for 3 average retinal illuminance levels of 10, 100, and 1,000 td. —, the fits of a quasi-linear model described in the text.

quency and decreasing retinal illuminance (Fig. 2, *A–C*, *bottom traces*). The phase response inflection at mid-frequencies was characteristic of the resonance phenomenon, showing little inter-cell variation.

Quasi-linear model described in the APPENDIX are shown by —. The model cascaded groups of first- and second-order linear filters of varying time constants. There were four free parameters: the time constant τ_1 of a first-order filter, the time

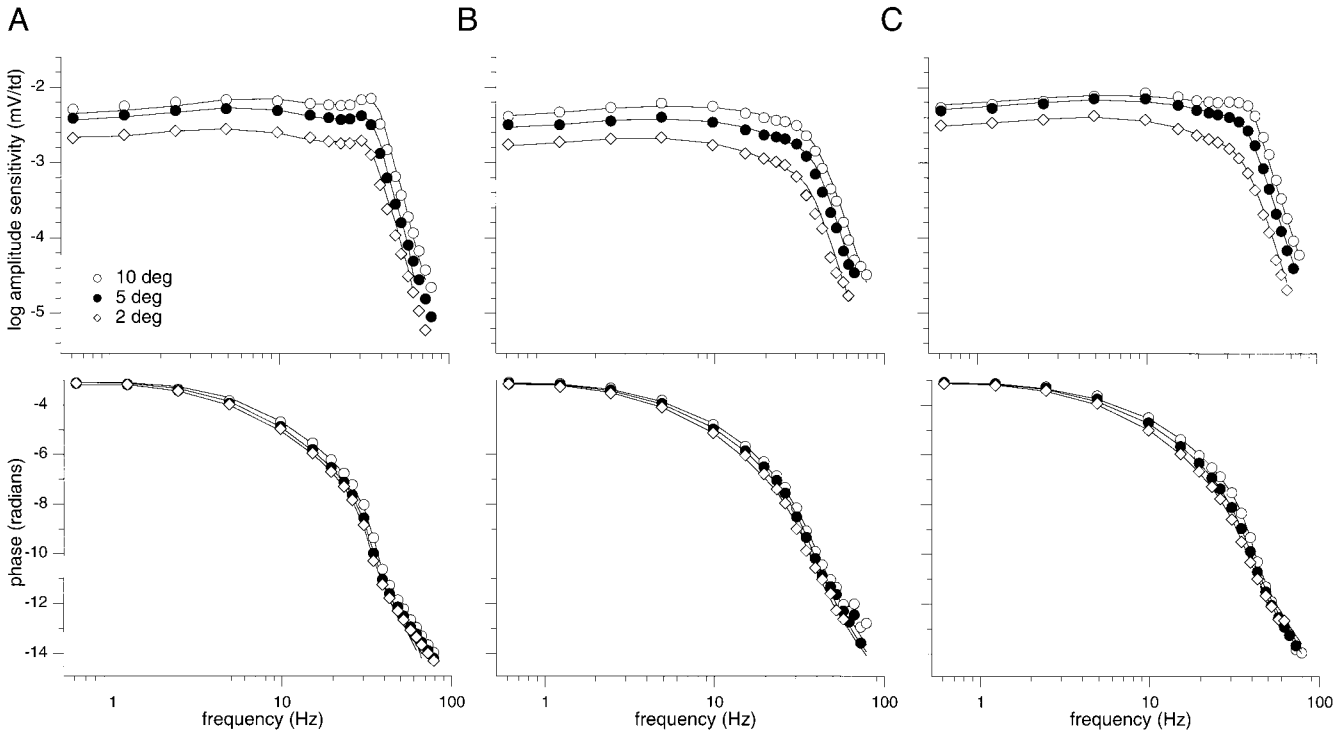

FIG. 3. Amplitude sensitivity (*top traces*) and phase (*bottom traces*) plotted as a function of temporal frequency at 1,000 td average luminance for 3 H1 cells (*A*, *B*, and *C*). Data are shown for stimulus diameters of 10, 5, and 2°. —, the fits of the quasi-linear model.

TABLE 1. *Model fitting parameters for H1 cell responses to temporal sinusoids and pulse increment*

Fits to Fig. 2	Parameter	Time-Average Illuminance 1,000 td	100 td	10 td
Cell a	τ 1	3.8	13.2	45.0
	τ 2	4.0	4.6	5.0
	ξ	0.12	0.12	0.17
	sensitivity*	0.005	0.032	0.130
Cell b	τ 1	3.4	12.9	44.3
	τ 2	4.1	4.4	4.5
	ξ	0.14	0.26	0.53
	sensitivity	0.006	0.035	0.162
Cell c	τ 1	1.9	6.97	24.6
	τ 2	4.24	4.6	5.0
	ξ	0.24	0.22	0.32
	sensitivity	0.010	0.059	0.273
Fits to Fig. 3	Parameter	Stimulus Diameter 10°	5°	2°
Cell a	τ 1	3.6	5.9	7.8
	τ 2	4.6	4.8	4.9
	ξ	0.11	0.13	0.13
	sensitivity*	0.005	0.004	0.002
Cell b	τ 1	4.3	7.8	11.4
	τ 2	4.1	4.2	4.4
	ξ	0.3	0.25	0.26
	sensitivity	0.004	0.28	0.16
Cell c	τ 1	2.8	4.8	8.9
	τ 2	4.0	4.1	4.3
	ξ	0.15	0.22	0.27
	sensitivity	0.006	0.005	0.003
Fits to Fig. 6	Parameter	Steady Illuminance 100 td	10 td	1 td
	τ 1	8	23	58
	τ 2	4	5	5
	ξ	0.18	0.20	0.45
	sensitivity**	0.035	0.136	0.316

* Asymptotic sensitivity (gain); units are mV/trolands (td). ** Sensitivity units are R_{max}/I_{sat}.

constant τ_2 of a three-stage first-order cascade, the under-damping constant ζ of a second-order filter, and a scaling constant. The scaling constant was determined individually at each illuminance level. The quality of the fits was good, with minor inter-cell variation. The values of the parameters for the cells of Fig. 2 are shown in Table 1. The data for lower illuminances could be fit with variation in the time constants of the filters, the under-damping constant, and the scaling constant. We noted in particular that the mid-frequency slope required adjustment of only one first-order filter, τ_1 (Table 1). This time constant lengthened as retinal illuminance decreased, from 3–5 ms at 1,000 td to 30–50 ms at 10 td. In comparison, the three-stage first-order cascade and the underdamping, ζ of the second-order filter changed little; τ_2 and ζ were near 4 ms and 0.13 at 1,000 td, and 5 ms and 0.3–0.4 at 10 td.

Stimulus area

We next investigated the temporal modulation properties of horizontal cells as a function of stimulus area at the highest retinal illuminance level (1,000 td). Stimulus diameters ranged between 2 and 10°. The methods were those described in the preceding text. The data sample included nine cells measured at two or more stimulus diameters and five cells measured at 10°. Amplitude sensitivity was calculated from the Fourier first-harmonic amplitudes and the slope of the contrast response function as described in the preceding text. Amplitude sensitivity and phase (estimated from the 0.25 Michelson contrast data) are plotted as a function of temporal frequency for three H1 cells in Fig. 3. Amplitude sensitivity increased with increase in area. Eleven of the 14 cells tested at 10° showed clear resonance with a peak near 40 Hz. As area was decreased, the resonance tended to decrease, although with variability among cells. The phase data were similar to those of Fig. 2 and showed a minor change with area. A phase advance occurred in the mid-frequency range as area increased. This advance reflects the increasing underdamping of the resonance filter. The cell in Fig. 3*A* showed pronounced resonance that changed little with area; the cell in Fig. 3*B* showed moderate resonance at all areas, and the cell in Fig. 3*C* showed a clear decrease in resonance with decrease in area. The data were well fit by the quasi-linear model described in the APPENDIX. The variations in underdamping evident in the data were obvious in the fit parameters. A less obvious change was a 2.5-fold increase in the τ_1 fitting constant as area decreased from 10 to 2°. The fitting parameter values for the cells of Fig. 3 are included in Table 1.

Responses to pulses

Pulse data were obtained from 12 H1 cells using steady backgrounds of 1–100 td and a 5° diam stimulus. There was some inter-cell variability in sensitivity but little variation in the shape of the responses.

Figure 4 shows averaged responses to a 10-ms pulse for one H1 cell for Weber contrasts of 0.1 to 16; Fig. 5 shows a parallel plot for the 100-ms pulse data. Each background retinal illuminance is shown in a separate panel. Light pulses evoked hyperpolarizing responses for all contrasts and backgrounds. As Weber contrast increased, response amplitude increased but did not saturate even at the highest contrast and highest retinal illuminance. The shape of the responses changed little with Weber contrast, which acted primarily to scale response height. Cells varied in sensitivity. Summary statistics of the response amplitude and the response latency at the peak response are shown in Table 2 for a Weber contrast of 19.

The time-to-peak for the 10-ms pulses varied little with background level. In comparison, time-to-peak for the 100-ms pulses lengthened as the background level decreased. After a rapid hyperpolarization in the first 40 ms, the response amplitude continued to increase more slowly to its peak. These data are consistent with the sine-wave data in showing activity of an illuminance-dependent time constant. The pulse response at 10 ms oscillated, most strongly at the highest background level. Oscillation was less evident in the 100-ms data. The oscillation frequency was similar (30–40 Hz) to that at which the resonance peak or shoulder occurred in the sine-wave temporal response. For the 100-ms pulse, there was a repolarizing sag following the peak hyperpolarization; additionally, there was a depolarizing aftershoot at light offset on the 100-td background.

The inner segment voltage response of isolated cones, mea-

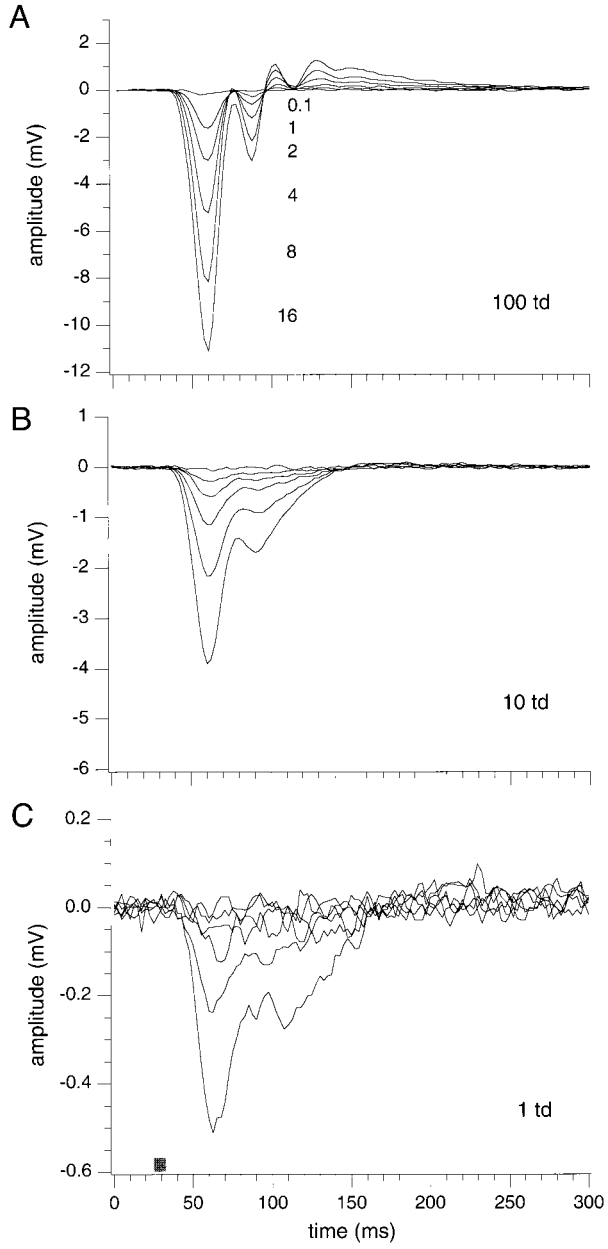

FIG. 4. H1 cell responses to 10-ms pulses at 6 Weber contrasts (0.1, 1, 2, 4, 8, and 16). Stimulus diameter was 5° and background retinal illuminances were 100 td (*A*), 10 td (*B*), and 1 td (*C*). ▤, stimulus duration.

sured with a 10-ms pulse showed a peak response latency of 32 ± 7 ms (Schneeweis and Schnapf 1999). The average latency for H1 cells was about 4 ms longer, reflecting the added processing of synapse and H1 cell receptor; this result is consistent with the average time constants of about 4–5 ms/stage in fitting the sine wave data (Table 1). The isolated cone data (Schneeweis and Schnapf 1999) showed no change in dynamics as background level increased.

At higher pulse contrasts, we expected to find contrast-dependent non-linearities. The pulse stimuli represent much higher contrasts than are obtainable with sine-wave stimulation. Indeed, we noted in the 10-ms responses that the oscillation was greater at the highest pulse level (Weber contrast of 19) than predicted by scaling the lowest pulse level. There were also subtle timing changes for the 10-ms pulse at the highest background. We noted a small but systematic decrease in peak response latency.

Figure 6 shows raw traces of responses to illuminance pulses of 10, 100, and 160 ms at a fixed Weber contrast of 8 for the same H1 cell as shown in Figs. 4 and 5. The data for different durations showed good temporal superposition, indicating that the initial hyperpolarizing response is linear. A simulation of the hyperpolarization based on the quasi-linear model described in the APPENDIX is shown by —. The parameter values are included in Table 1. These were within the range of those fitted to the sinusoidal data. With decrease in background illuminance, the time constant, τ_1 of the first-order linear filter increased from 8 to 58 ms, the time constant, τ_2 of the three-stage first-order cascade increased from 4 to 5 ms, and the underdamping constant, ζ of the second-order filter increased

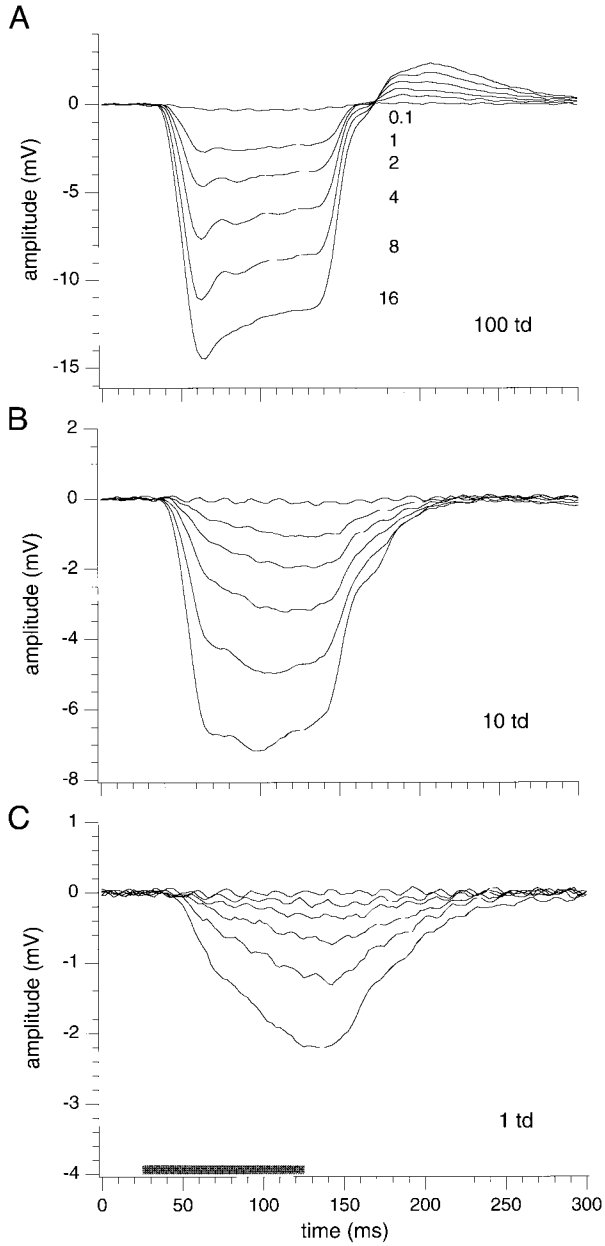

FIG. 5. Responses to 100-ms pulses at the 6 Weber contrasts for the same H1 cell as shown in Fig. 4. Stimulus diameter was 5° and background retinal illuminances were 100 td (*A*), 10 td (*B*), and 1 td (*C*). ▤, stimulus duration.

TABLE 2. *Summary data for H1 cell responses to pulse stimuli at a Weber contrast of 19 for three steady illuminances*

No. of Cells	Pulse Duration, ms	Steady Illuminance, td	Average Response Amplitude, mV	Latency at Peak Response, ms
12	10	100	13.97 ± 2.45	36.35 ± 2.70
		10	4.31 ± 0.57	39.55 ± 2.70
		1	0.52 ± 0.10	42.70 ± 3.45
9	100	100	19.38 ± 3.80	45.80 ± 4.68
		10	8.43 ± 1.37	58.33 ± 10.90
		1	1.85 ± 0.61	101.67 ± 18.41

Values are ±SD.

from 0.18 to 0.45. In particular, as retinal illuminance was decreased one time constant lengthened to describe the slow increase in response amplitude characteristic of the data. The linear model thus can describe the H1 cell data in both the frequency and the time domain.

Stimulus area

Figure 7 shows responses of another H1 cell to 10-ms pulses at four Weber contrasts (1, 2, 4, and 9) on a steady background of 130 td. Four diameters ranging from 1 to 15° are shown in *A–D*. The peak response hyperpolarization increased with field diameter. Oscillatory responses were evident at the 4° diam and became very pronounced for the 15° diam with a period of 28 ms. The latency of the peak hyperpolarization was shortest for the largest diameter, consistent with an increase in underdamping of a resonant filter. These data paralleled the effect of area on the temporal amplitude sensitivity functions, showing a shallow summation function. Probably the smallest field (1°) covers the summation area for direct inputs to H1 cell dendrites from the L and M cones. Summation between 1 and 4° therefore reflects the summation properties of the H1 cell coupled network. The 15° field probably exceeds the summation area of the coupled network.

Sensitivity regulation

A major goal of our study was to estimate sensitivity regulation in the outer retina of the primate. Both the sinusoidal and the pulse protocols can be used to estimate sensitivity regulation as a function of retinal illuminance level once the data are expressed in identical units of amplitude sensitivity (response amplitude in mV divided by stimulus amplitude in td). For sinusoidal data, amplitude sensitivity is estimated from the linear fits of the Michelson contrast data (Fig. 1) at low temporal frequency. For pulse data, amplitude sensitivity was estimated from parameters ($\Delta V_{max}/I_{sat}$) of the saturation functions fit to the pulse illuminance data (as described in the following text). We wanted a robust estimate of the sensitivity regulation in the H1 cell. The protocol to obtain the temporal amplitude sensitivity functions was lengthy, and there was a possibility that recording quality and thus sensitivity would vary over the data collection period. We therefore designed an abbreviated protocol to collect sinusoidal and pulse data and obtained full data sets on 12 cells. Sinusoidal data were collected at 0.61 Hz and 0.125 Michelson contrast at fixed steady illuminations (10–1000 td). We also obtained data at 19.52 Hz using a dynamic protocol (Lee et al. 1999). A 19.52-Hz test wave was superimposed on a 0.61-Hz vehicle wave. In this report, we present only the test data sampled at the maximum illumination level of the vehicle wave; these data were identical to data collected at matched steady illumination. The pulse protocol was as described in the preceding text. The sinusoidal and pulse protocols were run at different but overlapping ranges of steady illumination. To the extent that they yielded similar estimates of sensitivity change, we can be assured that the assumption of linearity of our measurement was robust. In this regard, the good agreement of the temporal dynamics for the two protocols (Table 1) was reassuring.

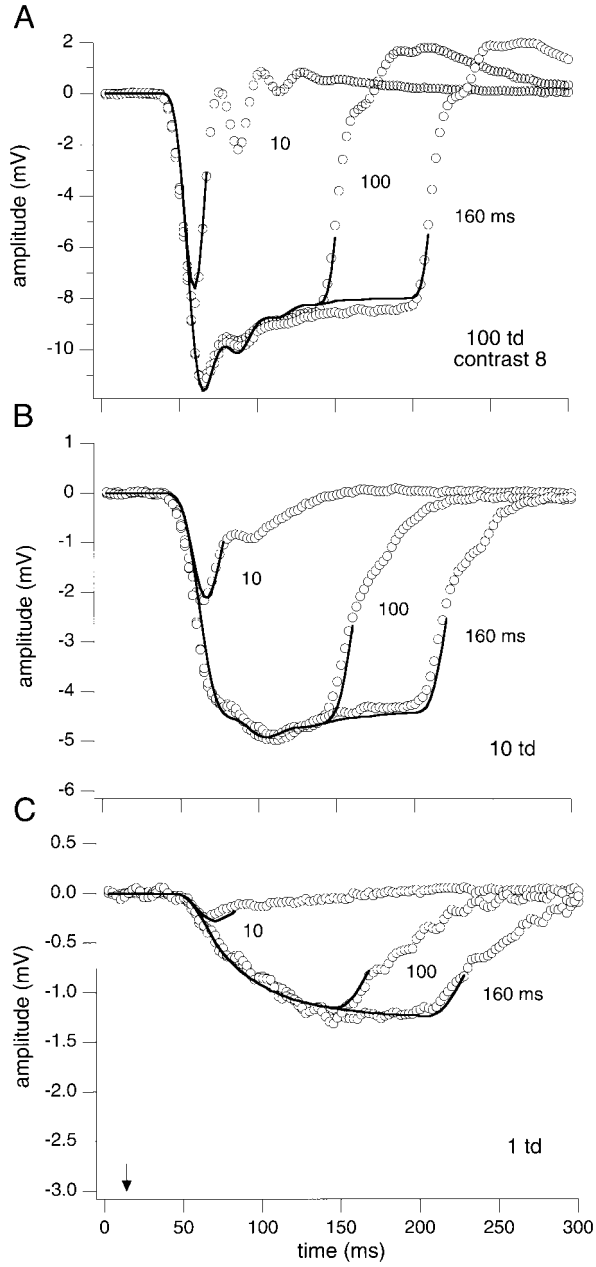

FIG. 6. Responses at 3 different pulse durations (10, 100, and 160 ms) to a fixed Weber contrast of 8 for the same H1 horizontal cell as shown in Figs. 4 and 5. Stimulus diameter was 5° and background retinal illuminances were 100 td (*A*), 10 td (*B*), and 1 td (*C*). ○, the data; —, fits of the simulation of the pulse response using the quasi-linear model described in the APPENDIX. ↓, stimulus onset.

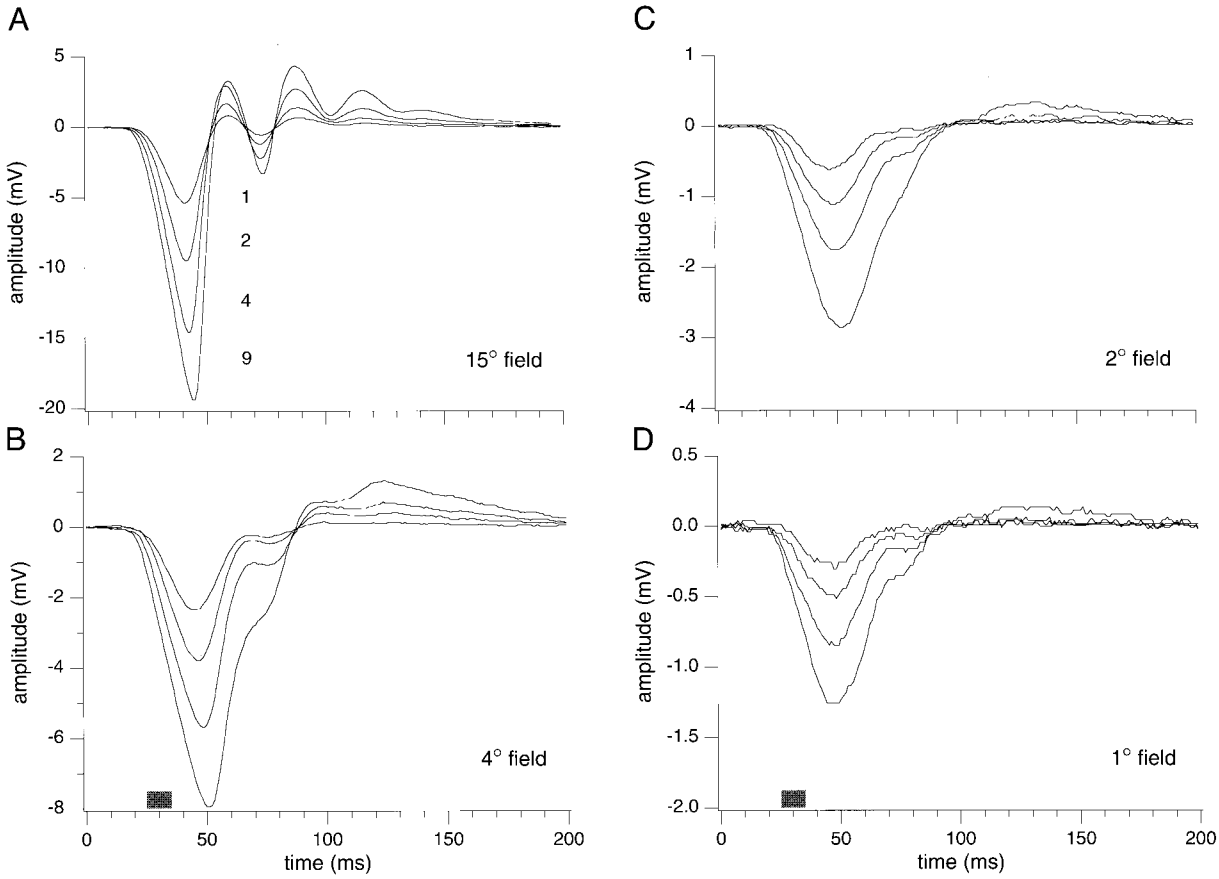

FIG. 7. Effect of stimulus area. Responses of an H1 horizontal cell to 10-ms pulses at 4 Weber contrasts (1, 2, 4, and 9) and a background illuminance of 316 td. Stimulus diameters were 15° (*A*), 4° (*B*), 2° (*C*), and 1° (*D*).

In the absence of neural regulation, sensitivity is mediated solely by the saturation function of the cone (Hood and Finkelstein 1986). At each steady-state luminance, sensitivity to light increments is assessed on a higher point of this saturation function, thus reducing the available response range. This phenomenon is called response range compression. In comparison, a neural mechanism of sensitivity regulation shifts the characteristic saturation function on the luminance axis. When sensitivity regulation obeys Weber's Law, the shift exactly compensates for the increase in steady-state illuminance; amplitude sensitivity is accessed at the foot (or threshold) of the shifted saturation function and should decline inversely with steady-state illuminance. Neural sensitivity regulation that does not reach Weber's law shifts the saturation function a lesser amount. Amplitude sensitivity should show the effects of both the partial sensitivity regulation (the shift) and the resultant response range compression (measurement on the rising portion of the shifted saturation function) (Normann and Anderton 1983; Normann and Perlman 1979; Valeton 1983).

Figure 8 shows the peak hyperpolarization amplitudes for the 10- and 100-ms pulse responses shown in Figs. 5 and 6, plotted as a function of pulse retinal illuminance. Data for the three steady retinal illuminances (1, 10, and 100 td) are shown with data for the 100-ms pulse in Fig. 8*A* and data for the 10-ms pulse in Fig. 8*B*. As background level was increased, the response amplitude for the 100-ms pulse was less at a matched pulse illuminance; the three data sets were displaced on the illuminance axis. This behavior is indicative of response range compression and/or neural sensitivity regulation (Normann and Anderton 1983; Normann and Perlman 1979; Valeton 1983). We did not collect enough low contrast data to evaluate the linear range of the response ($\Delta V_{max}/I_{sat}$) on bright backgrounds. The — are fits of the Michaelis-Menten saturation equation applied to increment responses

$$\Delta V_{inc} = \Delta V_{max} I_{inc}/(I_{inc} + I_{sat}) \quad (1)$$

where ΔV_{inc} is the response amplitude (mV) measured from resting level to the peak hyperpolarization, ΔV_{max} is the maximal increment hyperpolarization for the cell, I_{inc} is the pulse retinal illuminance, and I_{sat} is the illuminance at which the response is half ΔV_{max}. In this equation for increment pulses, both ΔV_{max} and I_{sat} vary with the steady illumination. However, we noted that the estimate of ΔV_{max} was only well constrained at the highest (100 td) steady adapting level, where the response amplitude increased rapidly with pulse illuminance. Since amplitude sensitivity depends only on the slope ($\Delta V_{max}/I_{sat}$) of the saturation function, we can fit all three data sets simultaneously, requiring one value for ΔV_{max} and individual values for I_{sat} at each steady level. With a 100-ms pulse, ΔV_{max} was 21 mV; the values of I_{sat} at 1, 10, and 100 td were 124, 258, and 645 td, respectively. The amount of sensitivity adjustment between 10 and 100 td (~2.6-fold) was below that predicted by Weber's law (10-fold). With a 10-ms pulse, data for 1-and 10-td backgrounds fell on the same saturation function (ΔV_{max} of 19 mV, I_{sat} of 561), but data for the 100-td background were displaced to higher illuminances (I_{sat} of 973

td). At low adaptation levels, responses were in the linear range of *Eq. 1* for several contrasts. We therefore checked the adequacy of the fits by evaluating these linear slopes to obtain a direct estimate of ($\Delta V_{max}/I_{sat}$). This second analysis gave estimates that were within the variability of the data.

The sinusoidal data at 0.61 Hz and the 100-ms pulse data are both estimates of the steady-state response of the cells. The 100-ms pulse duration exceeded critical duration for all three adaptation levels. The amplitude sensitivity data from the two protocols may therefore be compared. The joint data give an extended range of illuminance from 1 to 1,000 td and retinal illuminances of 10 and 100 td provided overlapping estimates of sensitivity. Figure 9 shows average (±1 SD) amplitude sensitivity for all 15 cells plotted as a function of background or time average retinal illuminance in a double logarithmic format. Data from the pulse protocol are shown as open symbols; sine-wave data are shown as closed symbols. Data for the 0.61 Hz sine-wave and the 100-ms pulses overlapped, indicating that the sinusoidal and pulse protocols gave similar estimates of sensitivity regulation. Sensitivity decreased with increase in retinal illuminance. The change in sensitivity did not achieve Weber's law. The slope near 1,000 td was approximately −0.65 to −0.7. Thus our data were consistent with a neural mechanism that provided square root sensitivity regulation near and above 100 td.

At shorter durations or at higher frequencies, there was evidence of time-dependant sensitivity regulation. The 19.52 Hz sine-wave data were less sensitive at 10 td but converged on the 0.61 Hz data by 1,000 td as noted also in the temporal amplitude sensitivity data of Fig. 2. In Fig. 9*C* we compare the data for 10 and 100 ms. The 10-ms pulses showed an asymptote near 10 td to a lower sensitivity than the 100-ms pulse data that continued to increase in sensitivity between 1 and 10 td. Both sets of data indicated that as retinal illuminances dropped below 100 td, the increase in sensitivity was achieved by a change in dynamics. The modeling indicated that only one time constant in the cascade was required to predict this added sensitivity. The other time constants changed to only a minor degree in the fits (Table 1).

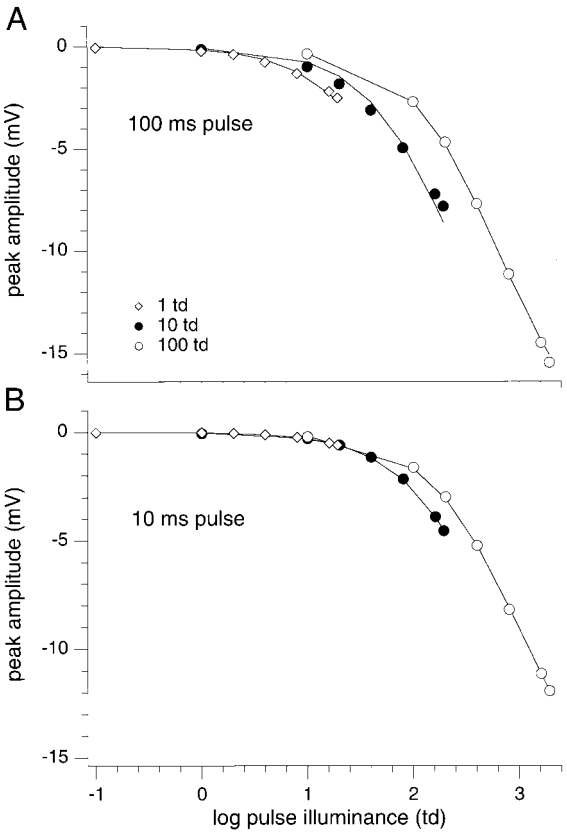

FIG. 8. Peak response amplitudes of Figs. 4 and 5 plotted as a function of pulse luminance at three retinal illuminances (1, 10, and 100 td). Pulse durations were 100 (*A*) and 10 ms (*B*). —, fits of the Michaelis-Menten equation as explained in the text.

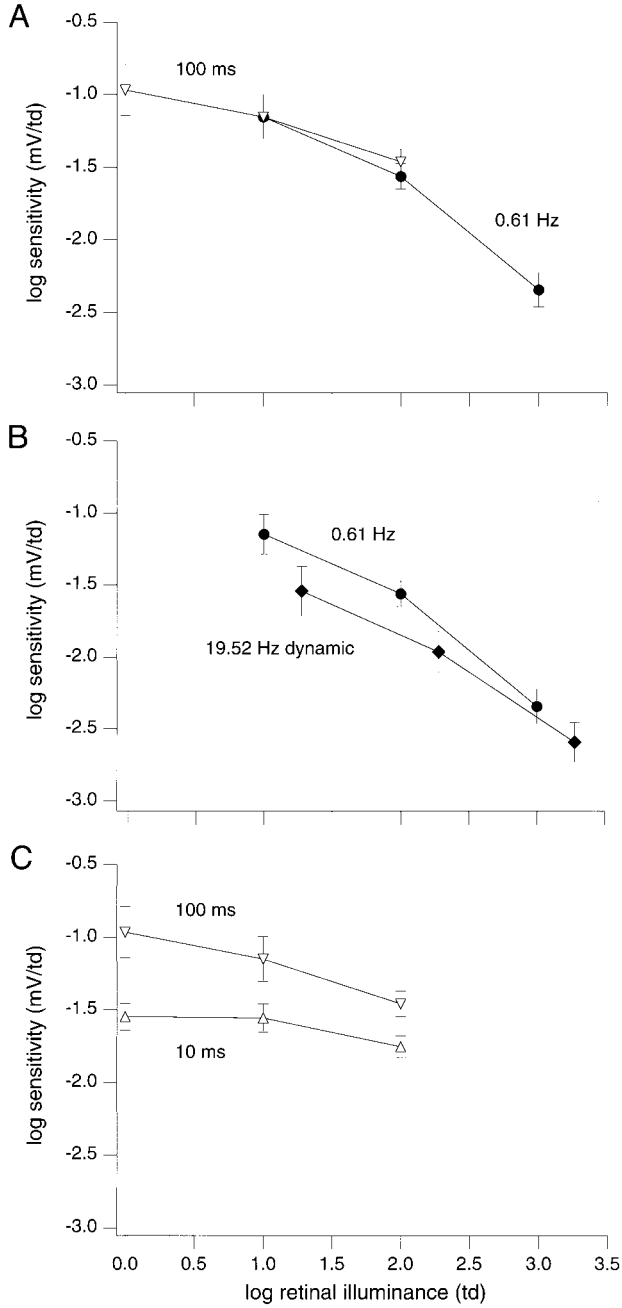

FIG. 9. Average amplitude sensitivity (mV/td) for 15 H1 horizontal cells plotted as a function of the time average (sine-wave data) or the background (pulse data) retinal illuminance. *A*: compares responses to a 0.61-Hz sine-wave stimulus (●), with 100-ms pulses (▽). *B*: compares the 0.61-Hz with the 19.52-Hz sine-wave stimulus (♦). *C*: compares the 10- and 100-ms pulses.

It is useful to estimate how much of the sensitivity loss can be attributed to response range compression. Normann and Perlman pointed out that the parameters ΔV_{max} and I_{sat} for increment data (*Eq. 1*) are related to parameters V_{max} and σ used in the Michaelis-Menten equation for total incident light ($I_B + I_{inc}$) by equations

$$\Delta V_{max} = V_{max}(1 - I_B/(I_B + I_{sat})) \quad (2)$$

$$\sigma = I_{sat} - I_B \quad (3)$$

where I_B is the background retinal illuminance, V_{max} is the maximal response range of the cell and σ is the illuminance at half V_{max} measured by increments in dark-adapted conditions, or by combining maximal increment and decrement responses in light-adapted conditions. Previous studies of cone photoreceptors (Normann and Anderton 1983; Normann and Perlman 1979; Valeton and van Norren 1983) concurred that the maximal response range, V_{max}, changed little with light level, but Burkhardt (1994) noted a decrease in V_{max} at and above bleaching levels. The sensitivity loss in the light-adapted condition (ΔS_L) relative to the dark-adapted sensitivity (ΔS_D) is the product of the neural gain and response compression factor (Normann and Anderton 1983). It is given by

$$\Delta S_L/\Delta S_D = G(I_B)(V_{max}/(V_{max} - I_B/(I_B + \sigma)))^2 \quad (4)$$

where I_B and $G(I_B)$ are the retinal illuminance and neural gain at background, *B*, and

$$\Delta S_D = V_{max}/\sigma \quad (5)$$

Response range compression was evident above 150 td and showed an asymptote near 0.4 at 100,000 td in primate cones (Valeton and van Norren 1983). Response range compression showed an asymptote near 0.5 in turtle cones (Burkhardt 1994; Normann and Anderton 1983).

We separately estimated response compression in three cells by the use of decrement pulses on steady backgrounds and verified that *Eqs. 1–4* could be used to estimate response compression from increment data. We then calculated the effect of response compression in the cells of Fig. 9. We noted no evidence of response range compression at 1 td. Response range compression decreased sensitivity by 0.01 log unit at 10 td and 0.08–0.10 log unit at 100 td. Thus our estimate of response range compression in individual primate H1 cells was similar to that reported by Valeton and van Norren (1983) using mass recording in primate outer retina.

Figure 10 shows a comparison of relative sensitivity for our data (left ordinate), and estimates from electroretinogram (ERG) (Valeton and van Norren 1983) and single cones (Schneeweis and Schnapf 1999) (right ordinate). Data for 0.61-Hz sine-wave stimuli and 100-ms pulses are shown in Fig. 10*A* as △—△ and ●—●. Data for the 10-ms pulses are shown in Fig. 10*B*. Calculations of the amount of sensitivity regulation contributed by bleaching or by sensitivity regulation and response compression in the photoreceptor are shown by —. These calculations use the authors' published estimates of trolands. The bleaching effect was calculated on the basis of published isomerization values (Wyszecki and Stiles 1982). The mass recording photoreceptor gain, based on the 500-ms data (Valeton and van Norren 1983), is shown in Fig. 10*A* for comparison with the 100-ms H1 cell data. The single-unit photoreceptor gain, based on the 10-ms data for macaque inner segments (Schneeweis and Schnapf 1999), is shown in Fig. 10*B* for comparison with the H1 cell 10-ms data.

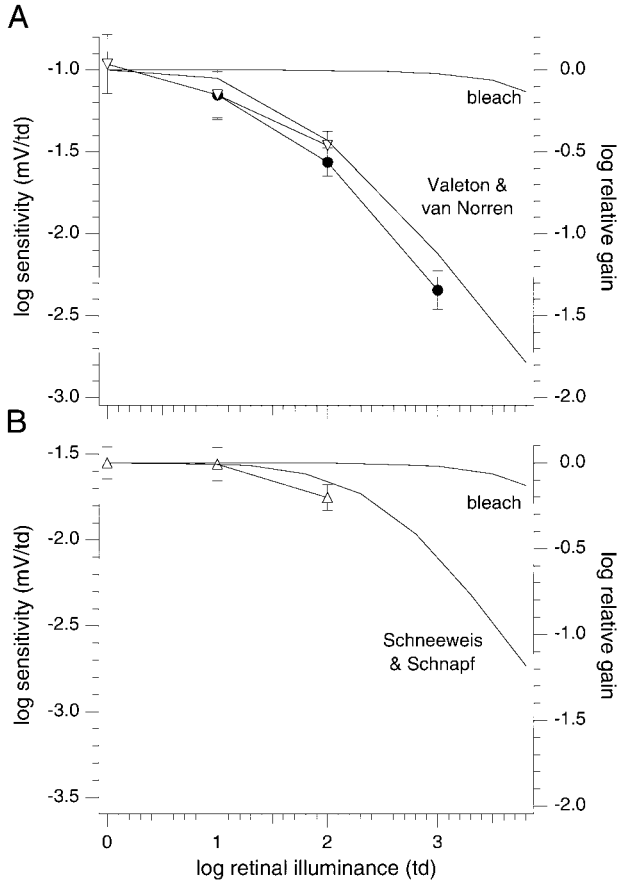

FIG. 10. Comparison of amplitude sensitivity for 15 H1 horizontal cells with literature data. *A*: the average sensitivity gain from Fig. 9 for 0.61-Hz sine-wave stimuli and 100-ms pulses is replotted on the left ordinate. Calculations of the expected bleaching effect and the sensitivity gain calculated from the Valeton and van Norren (1983) mass recording of photoreceptor gain are plotted as solid curves on the right ordinate. *B*: average sensitivity gain from Fig. 9 for 10-ms pulses is replotted on the left ordinate. Calculations of the expected bleaching effect and the sensitivity gain calculated from the Schneeweis and Schnapf (1999) single-unit recording of photoreceptor gain are plotted as — on the right ordinate.

In Fig. 10*A*, it is clear that neural sensitivity regulation was in operation at least 3.0 log units below bleaching effects. Our 100-ms data showed gain adjustment initiated between 1 and 10 td, a lower illuminance than Valeton and van Norren (1983). Our 10-ms data (Fig. 10*B*) show sensitivity adjustment between 10 and 100 td, a lower illuminance than Schneeweis and Schnapf (1999).

DISCUSSION

Linearity of H1 cell data

Psychophysical threshold data are often assumed to obey small signal linearity, and we fit our sinusoidal data at each adaptation level using a linear systems approach. The dynamics of the initial hyperpolarization of the pulse data could also be described by a linear model with dynamics similar to those used for the sinusoidal data. Both sinusoidal and pulse data gave parallel estimates of the change in temporal dynamics and similar estimates of the illumination range for sensitivity reg-

ulation. Thus the response properties we estimated from H1 cell responses were reasonably linear and well-behaved, supporting the notion that the initial portion of the response reflects linear response behavior of photoreceptors and H1 cell.

Comparison with non-primate mammalian data

The H1 cell temporal sensitivity was similar to that derived from the cat horizontal cells (Foerster et al. 1977; Lankheet et al. 1989a,b, 1991a,b). In cat, recordings were typically obtained from the B-type, axon-bearing horizontal cell, which corresponds morphologically to the primate H1 cell type (Boycott et al. 1978). The temporal frequency response for cat H1 cells was low-pass with resonance at 30–40 Hz. Sensitivity regulation was evident about 1 log unit above threshold for the cat. Weber's law was not obtained; the limiting slope was 0.64. Lankheet et al. (1993) hypothesized that the neural sensitivity regulation obeyed a square root law and that response range compression accounted for the steepening slope at higher adapting luminances.

Comparison with other primate data

There are two major studies that give estimates of primate cone light sensitivity regulation that can be compared with our results in H1 cells. Our 0.61-Hz/100-ms data showed H1 cell sensitivity regulation at lower retinal illuminances than Valeton and van Norren's (1983) massed recordings of the outer segment layer in the fovea. In general, there was substantial agreement in the slopes of the data sets. Our estimates of response compression are similar to theirs. The discrepancy is primarily in the sensitivity axis and may arise from the extensive spatial averaging characteristic of mass recording technique.

Our 10-ms H1 cell data showed sensitivity regulation at lower retinal illuminances than the Schneeweis and Schnapf (1999) whole cell voltage recordings from cone inner segments. One source of the discrepancy may lie in the calibration of the troland axis. Estimates of light level are subject to error and can vary by a half log unit or more among laboratories (Hood and Birch 1993). In the Schneeweis and Schnapf study, recordings were made from pieces of retina placed as a flat mount in a recording chamber. The calculation of equivalent retinal illuminance involves assumptions about the effective light collecting ability of the photoreceptors. We allowed a sixfold factor for this compared with Schnapf et al. (1990), who allowed a threefold factor. Thus some of the discrepancy may lie in the troland level estimates. A second source of discrepancy may lie in differences between the preparations. In the in vitro preparation, the retina is attached to the pigment epithelium and can be maintained continuously at high photopic light levels, allowing H1 cells to be light- and dark-adapted over a period of hours (Verweij et al. 1999). Retinal ganglion cells show similar responsivity in the in vitro as in an in vivo preparation (Dacey and Lee 1994; Lee et al. 1990). In comparison, measurements of the inner segment voltage response used pieces of retina detached from the retinal pigment epithelium (Schneeweis and Schnapf 1999). Schneeweis and Schnapf (1999) remarked on considerable variability among individual cones. The most sensitive cone in their sample lay within the response variation of the H1 cells in the present study.

Non-linearities

Non-linearities were evident in both the sinusoidal and pulse data at high contrasts. The low-frequency harmonic distortion demonstrated in Fig. 1*A* can be obtained by a variety of non-linear operations. Similar low-frequency distortions in cat (Lankheet et al. 1993) were ascribed to an adaptational nonlinearity such as divisive feedback. Although divisive feedback can provide a description of the waveform, it predicts a decrease in the peak hyperpolarization relative to the offset depolarization. However our data showed the reverse, the offset depolarization accelerated relative to the peak hyperpolarization with increasing contrast (Fig. 1), suggesting other non-linearities. Pulse data were expected to show non-linearities due both to the higher contrast levels and to the activation of ion channels in the cone inner segment and/or in the H1 cell. The linear model captured the light-evoked hyperpolarization at 100 td but not the form of the pulse responses at pulse offset. There was a slow depolarization and delayed overshoot evident and, for longer pulses, the oscillation became less evident. The data did not return promptly to the zero baseline as predicted by the time constants of the linear model.

Conclusions

Sensitivity at low light levels (1 troland) showed a slowing in temporal dynamics, indicating time-dependent sensitivity regulation. Both the sinusoidal and the pulse data revealed changes in response dynamics with changes in retinal illuminance. The effect of these changes would be increased temporal summation at low luminances. We modeled this effect using the simulation and noted a change in critical duration from about 30 ms near 1,000 td to about 100 ms at 1 td. This range is comparable to that seen in human psychophysical data (Graham and Kemp 1938; Herrick 1956). In a companion study (Lee et al. 1999), we have shown that despite convergence of hundreds of L and M cone inputs to the large H1 cell receptive field, desensitizing one of the cone types did not affect the sensitivity of the other type. Further, sensitivity regulation could be measured locally in a small part of the H1 cell receptive field. This cone-type specificity is consistent with a cone photoreceptor locus for H1 cell adaptation at the higher portion of our illuminance range. Nonetheless we cannot definitively conclude that the sensitivity regulation we measured in H1 cells is entirely within the photoreceptor. It is possible that activity in the cone-H1 synapse can play a role in sensitivity regulation that could appear photoreceptor-specific.

Sensitivity was reduced at light levels above approximately 10 trolands, reflecting both response range compression and neural gain control. The H1 cell data never approached Weber's law even at 100 and 1,000 td. Other studies concur that sensitivity regulation in the cone photoreceptor does not produce Weber's law below bleaching levels. The non-mammalian vertebrate (Burkhardt 1994; Normann and Anderton 1983; Normann and Perlman 1979), the mammalian (Lankheet et al. 1993), and the primate (Valeton and van Norren 1983) have shown a combination of neural sensitivity regulation and response range compression. The data are consistent with slopes of 0.65–0.80 log unit of sensitivity regulation per decade of illuminance change until pigment depletion levels are reached. By contrast, Weber's law behavior can be measured below 10

td at the level of the retinal ganglion cell (Lee et al. 1990; Yeh et al. 1996). The more complete sensitivity reduction found for ganglion cells at this lower illuminance level is comparable to that observed in human psychophysical data. Thus it must be concluded that additional mechanisms of sensitivity regulation exist at the level of the bipolar and/or ganglion cell.

APPENDIX

Temporal sinusoidal responsivity data of cat retinal ganglion cells have previously been described by linear systems (e.g. Frishman et al. 1987; Victor 1987). We used this approach to derive a quasi–linear model of the H1 cell temporal frequency response.

Elements of the linear model

The fundamental temporal response is exponential, characterized by a time constant, τ (termed a first-order filter). Low-pass filters show reduced gain (ratio of output to input) and phase delay as frequency increases. A convenient way (Milsum 1966) to summarize temporal activity in the frequency domain is the Bode plot (output/input as a function of frequency) using logarithmic coordinates. We plot log amplitude versus log frequency together with a plot of phase versus log frequency. For a single low pass filter

$$\text{Log Amp} = \log(\text{Gain}) - 0.5\{\log[1 + (\omega\tau_i)^2]\} \quad (A1)$$

$$\text{Phase} = -\arctan(\omega\tau_i) \quad (A2)$$

where ω is frequency in radians per second and τ_i is the characteristic time constant. In the Bode plot for amplitude, there is a horizontal asymptote at low frequencies with the value given by the gain and a slope of -1 at high frequencies. A group of cells and synapses is treated as a cascade of such filters. The advantage of the Bode plot is that the response of a cascade is the addition of the log gains and phases of each filter. In the amplitude plot, the low-frequency asymptote is given by a lumped gain of all the filters and the high-frequency asymptote has a negative slope given by the sum of the filters.

It is common also to allow a pure delay, which adds only a phase term

$$\text{Phase} = -(\omega\tau_d) \quad (A3)$$

Although the pure delay is often handled by additional low-pass filters with small time constants (e.g. Victor 1987), we found it simpler to use *Eq. A3.* An example of a simple cascade with such a pure delay was the cone light response, estimated (Hood and Birch 1993) from the cone a-wave of the human ERG. This response postulated a three-stage cascade of first-order filters with a time constant of 2 ms plus an initial delay of 2 ms (Hood and Birch 1993). This estimate was a linear approximation, consistent with computational models of the light sensitive channel (Lamb and Pugh 1992).

Resonance is another feature of cell behavior. Resonance refers to an increase in amplitude and advance in phase near a characteristic or "resonant" frequency. Resonance is described by an under-damped, second-order filter, characterized by a resonant frequency, ω_n and a damping constant, ζ. The greater the underdamping, the greater the effect. The Bode plot is given by

$$\text{Log Amp} = \log(\text{Gain}) - 0.5\log\{[1 - (\omega/\omega_n)^2]^2 + (2\zeta\omega/\omega_n)^2\} \quad (A4)$$

$$\text{Phase} = -\arctan\{(2\zeta\omega/\omega_n)/[1 - (\omega/\omega_n)^2]\} \quad (A5)$$

The low-frequency asymptote is given by the gain, but the high-frequency asymptote has a slope of -2. Between these asymptotes and provided $\zeta < 0.707$, there is a peak response which increases as ζ decreases and is maximal near the resonant frequency.

The final element allowed in the quasi-linear model is the "lead-lag" element (e.g. Milsum 1966). The lead-lag was introduced to allow reduced amplitude accompanied by phase advance at low frequencies (Frishman et al. 1987). The H1 cell shows only a slight low-frequency roll-off at the highest retinal illuminances. The lead-lag filter is characterized by its frequency τ_1 and weight, α. The Bode plot is of the form

$$\text{Log Amp} = \log(\text{Gain}) + 0.5\{\log[1 + (\alpha\omega\tau_1)^2]\} - 0.5\{\log[1 + (\omega\tau_1)^2]\} \quad (A1)$$

$$\text{Phase} = \arctan(\alpha\omega\tau_1) - \arctan(\omega\tau_1) \quad (A2)$$

The low-frequency asymptote is the gain and the high-frequency asymptote is α (i.e. if $\alpha = 2$, there will be a 0.30 log unit roll-off).

In physiology it is impossible to measure "gain" as output/input since the units are not identical. We therefore set the gains of the filters at unity and used an arbitrary scaling constant to match the low-frequency asymptote of the data expressed in amplitude sensitivity. Since the physiological data are not linear with retinal illuminance, this sensitivity must be fit individually at each steady-state retinal illuminance and for each stimulus area. Thus the model should properly be considered quasi-linear.

The elements of the quasi-linear model are diagrammed in Fig. A1. The ordering of the elements is arbitrary. Further, this type of model offers no hint as to the origin of the various elements. It is not usual in the systems approach to assign specific mechanisms to the sections of the model. We can tentatively associate the first-order filters with the inner segment and synapse. The second-order filter may be a feature of the H-cell network since our sinusoidal data showed the resonance was most pronounced for large areas. The lead-lag was used to allow fits to the low-frequency roll-off (Frishman et al. 1987). This type of behavior may reflect time-dependent adaptation; however, there is no neural interpretation associated with the lead-lag filter.

Fixed elements of the model

1) Initial low-pass filters and fixed delay: We allowed a three-stage cascade of first-order low pass filters with a time constant of 2 ms (Hood and Birch 1993) and an initial delay of 2 ms. This choice was fixed in the model fits and was considered to represent the dynamics of the cone light response, as discussed in the preceding text.

2) The resonant frequency of second order filter was yoked to the time constant, τ_3 of the variable cascade (see following text). This approach reduced the number of free parameters in the fits.

3) The lead-lag element was fixed with a time constant of 0.08 s and weighting of 1.5 to give a maximal roll-off of about 0.18 log unit with

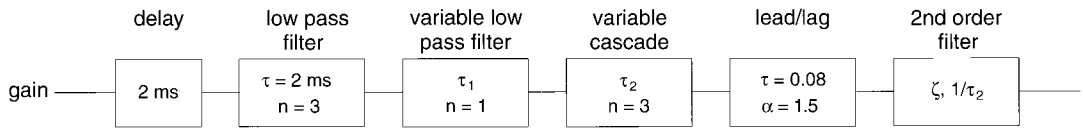

FIG. A1. Block diagram of the linear model, showing the delay, the low-pass, the lead/lag and second-order filters.

a maximal phase advance of 10°. The effect of the lead-lag element became evident at and below 5 Hz at the highest illuminances.

Variable elements of the model

There were four variable elements in the model: *1*) we allowed a single first-order filter with variable time constant, τ_1; *2*) we allowed a three-stage, first-order cascade with variable time constant, τ_2; *3*) we allowed a variable underdamping constant, ζ for the second-order filter; and *4*) we allowed a variable scaling constant (gain in Fig. A1) to match the model to the amplitude sensitivity/retinal illuminance at 0.61 Hz.

Fits were made using a least squares fitting procedure to first-harmonic amplitude and phase data expressed in the complex plane. The convergence of the fits was shallow. We checked the effect of varying the number of stages in the first-order cascade and found a trade-off of about 1 ms/stage between the number of stages and the time constant. The scaling parameter was not affected by this minor variation in the first- and second-order filters. Since optimal fits were usually obtained with a three-stage variable cascade, solutions are shown for this choice.

Model fits to pulse data

The sine-wave data were fit with a linear systems model. We used the fixed and variable first- and second-order linear filters to simulate the impulse response function for the linear filter model. The lead-lag element was not used. The impulse response function was then convolved with the pulse duration to see how well the simulated response captured the initial hyperpolarization of the pulse response. We did not expect such a model to fit the later stages of the response that may involve settling activity of ion channels in the inner segment of the photoreceptor and in the H1 cell. The pulse data at 100 and 160 ms showed a slow depolarization sag that obeyed temporal superposition. The sag could be modeled by negative feedback and this element was incorporated, as a fixed single stage low-pass filter with a time constant of 25 ms and feedback strength 0.4, so that the simulation described the entire hyperpolarizing portion of the response. Scaling constants ΔV_{max} and I_{sat} were used to scale the data at Weber contrasts 0.1–16.

A full optimization of the initial hyperpolarization with five free parameters was not feasible due to the noise of the data and subtle interactions among τ_1, τ_2, and ζ. We therefore used a grid search to find near-optimal values for these parameters that could describe the shape of the hyperpolarization. We then optimized ΔV_{max} and I_{sat}. We noted that a fixed value of ΔV_{max} (25–30 mV) could be used for all three illuminances.

We thank the Regional Primate Center at the University of Washington for primate tissue. We are especially grateful to T. Haun and K. Boro for technical assistance and to B. Peterson for preparation of the figures and editorial assistance.

This work was supported by grants from the National Eye Institute (EY-00901 and EY-06678), by support from the National Institutes of Health to the Regional Primate Center at the University of Washington, and by support from the Deutscheforschungsgemeinschaft (Le524/12-2).

REFERENCES

BOYCOTT BB, PEICHL L, AND WÄSSLE H. Morphological types of horizontal cell in the retina of the domestic cat. *Proc R Soc Lond B Biol Sci* 203: 229–245, 1978.

BOYNTON RM AND WHITTEN DN. Visual adaptation in monkey cones: recordings of late receptor potentials. *Science* 170: 1423–1426, 1970.

BURKHARDT DA. Light adaptation and photopigment bleaching in cone photoreceptors in situ in the retina of the turtle. *J Neurosci* 14: 1091–1105, 1994.

DACEY DM. Physiology, morphology and spatial densities of identified ganglion cell types in primate retina. *Ciba Found Symp* 184, 12–28; discussion 28–34, 63–70, 1994.

DACEY DM. Circuitry for color coding in the primate retina. *Proc Natl Acad Sci USA* 93: 582–588, 1996.

DACEY DM AND LEE BB. The 'blue-on' opponent pathway in primate retina originates from a distinct bistratified ganglion cell type. *Nature* 367: 731–735, 1994.

DACEY DM, LEE BB, STAFFORD DK, POKORNY J, AND SMITH VC. Horizontal cells of the primate retina: cone specificity without spectral opponency. *Science* 271: 656–659, 1996.

DONNER K, KOSKELAINEN A, DJUPSUND K, AND HEMILA S. Changes in retinal time scale under background light: observations on rods and ganglion cells in the frog retina. *Vision Res* 35: 2255–2266, 1995.

ENOCH JM AND LATIES AM. An analysis of retinal receptor orientation. II. Predictions for psychophysical tests. *Invest Ophthalmol* 10: 959–970, 1971.

FOERSTER MH, VAN DE GRIND WA, AND GRÜSSER O-J. The response of cat horizontal cells to flicker stimuli of different area, intensity and frequency. *Exp Brain Res* 29: 367–385, 1977.

FRISHMAN LJ, FREEMAN AW, TROY JB, SCHWEITZER-TONG DE, AND ENROTH-CUGELL C. Spatiotemporal frequency responses of cat retinal ganglion cells. *J Gen Physiol* 89: 599–628, 1987.

GRAHAM CH AND KEMP EH. Brightness discrimination as a function of the increment in intensity. *J Gen Physiol* 21: 635–650, 1938.

HERRICK RM. Foveal luminance discrimination as a function of the duration of the decrement or increment in luminance. *J Comp Psychol* 49: 437–443, 1956.

HOOD DC AND BIRCH DG. Human cone receptor activity: the leading edge of the a-wave and models of receptor activity. *Vis Neurosci* 10: 857–871, 1993.

HOOD DC AND FINKELSTEIN MA. Sensitivity to light. In: *Handbook of Perception and Human Performance. Sensory Processes and Perception*, edited by Boff KR, Kaufman L, and Thomas JP. New York: Wiley, 1986, vol. 1, p. 5-1–5-66.

LAMB TD AND PUGH EN JR. G-protein cascades: gain and kinetics. *Trends Neurosci* 15: 291–298, 1992.

LANKHEET MJM, MOLENAAR J, AND VAN DE GRIND WA. Frequency transfer properties of the spike generating mechanism of cat retinal ganglion cells. *Vision Res* 29: 1649–1661, 1989a.

LANKHEET MJM, MOLENAAR J, AND VAN DE GRIND WA. The spike generating mechanism of cat retinal ganglion cells. *Vision Res* 29: 505–517, 1989b.

LANKHEET MJ, PRZYBYSZEWSKI AW, AND VAN DE GRIND WA. The lateral spread of light adaptation in cat horizontal cell responses. *Vision Res* 33: 1173–1184, 1993.

LANKHEET MJ, VAN WEZEL RJ, AND VAN DE GRIND WA. Effects of background illumination on cat horizontal cell responses. *Vision Res* 31: 919–932, 1991a.

LANKHEET MJ, VAN WEZEL RJ, AND VAN DE GRIND WA. Light adaptation and frequency transfer properties of cat horizontal cells. *Vision Res* 31: 1129–1142, 1991b.

LATIES AM AND ENOCH JM. An analysis of retinal receptor orientation. I. Angular relationship of neighboring photoreceptors. *Invest Ophthalmol* 10: 69–77, 1971.

LEE BB, DACEY DM, SMITH VC, AND POKORNY J. Horizontal cells reveal cone type-specific adaptation in primate retina. *Proc Natl Acad Sci USA* 96: 14611–14616, 1999.

LEE BB, POKORNY J, SMITH VC, MARTIN PR, AND VALBERG A. Luminance and chromatic modulation sensitivity of macaque ganglion cells and human observers. *J Opt Soc Am A* 7: 2223–2236, 1990.

MACLEOD DI, WILLIAMS DR, AND MAKOUS W. A visual nonlinearity fed by single cones. *Vision Res* 32: 347–363, 1992.

MILSUM JH. *Biological Control Systems Analysis.* New York: McGraw-Hill, 1966.

NORMANN RA AND ANDERTON PJ. The incremental sensitivity curve of turtle cone photoreceptors. *Vision Res* 23: 1731–1733, 1983.

NORMANN RA AND PERLMAN I. The effects of background illumination on the responses of red and green cones. *J Physiol (Lond)* 286: 491–507, 1979.

PUGH EN JR AND LAMB TD. Cyclic GMP and calcium: the internal messengers of excitation and adaptation in vertebrate photoreceptors. *Vision Res* 30: 1923–1948, 1990.

SCHNAPF JL, NUNN BJ, MEISTER M, AND BAYLOR DA. Visual transduction in cones of the monkey *Macaca fascicularis. J Physiol (Lond)* 427: 681–713, 1990.

SCHNEEWEIS DM AND SCHNAPF JL. The photovoltage of macaque cones photoreceptors: adaptation, noise and kinetics. *J Neurosci* 19: 1203–1216, 1999.

SMITH VC, DACEY DM, LEE BB, POKORNY J, AND STAFFORD DK. Temporal contrast sensitivity and adaptation in primate horizontal cells (Abstract). *Invest Ophthalmol Vis Sci Suppl* 37: S6, 1996.

STILES WS. *Mechanisms of Colour Vision.* London: Academic, 1978.

VALETON JM. Photoreceptor light adaptation models: an evaluation. *Vision Res* 23: 1549–1554, 1983.

VALETON JM AND VAN NORREN D. Light adaptation in primate cones: an analysis based on extracellular data. *Vision Res* 23: 1539–1547, 1983.

VERWEIJ J, PETERSON BB, DACEY DM, AND BUCK SL. Sensitivity and dynamics of rod signals in H1 horizontal cells of the macaque monkey retina. *Vision Res* 39: 3662–3672, 1999.

VICTOR JD. The dynamics of the cat retinal X-cell centre. *J Physiol (Lond)* 386: 219–246, 1987.

WYSZECKI G AND STILES WS. *Color Science-Concepts and Methods Quantitative Data and Formulae* (2nd ed.). New York: Wiley, 1982.

YEH T, LEE BB, AND KREMERS J. Time course of adaptation following luminance and chromatic change. *Vision Res* 36: 913–931, 1996.